PAPER

Surface modification of banana stem fibers *via* radiation induced grafting of poly(methacrylic acid) as an effective cation exchanger for Hg(II)†

N. Salamun,[a] S. Triwahyono,*[ab] A. A. Jalil,[cd] Z. A. Majid,[a] Z. Ghazali,[e] N. A. F. Othman[e] and D. Prasetyoko[f]

A low cost adsorbent, banana stem fibers (BSFs), was used for modification by grafting with methacrylic acid *via* three free radical generation methods. The presence of poly(methacrylic acid) on the adsorbent surface was verified by FTIR, ESR and TG analyses. BSFs grafted *via* β-radiation (BSF-β) were proven to have a higher grafting yield which led to a higher Hg(II) adsorption capacity. A slight decrease in the equilibrium pH after the adsorption process was probably due to BSF-β acting as an acid-form ion-exchanger. The adsorption equilibrium uptake fitted well with the Freundlich isotherm model implying that Hg(II) adsorption occurred heterogeneously on the adsorption sites. The kinetics of adsorption follows a pseudo-first order model with an activation energy of 13.7 kJ mol^{-1} indicating that the adsorption undergoes an ion-exchange process. Thermodynamic studies illustrated that that the Hg(II) adsorption process was endothermic and non-spontaneous. Spent BSF-β was effectively regenerated with 0.1 M HCl and could be reused without any significance efficiency loss over at least six cycles of adsorption. The present investigation shows that BSF-β is a promising adsorbent for the removal and recovery of Hg(II) ions from aqueous solutions.

Introduction

Contamination of various water resources with heavy metals is considered as a serious problem because of their harmful and toxic effects on human health and living organisms. Therefore, it is of great interest to remove heavy metals from wastewater. Among the heavy metals, mercury is one of the most dangerous even at a low concentration. The major sources of mercury pollution are effluents from oil refining, pulp paper, chlor-alkali, electrical, rubber processing and fertilizer industries.[1,2] There are several methods so far that have been used for the removal of Hg(II) such as chemical precipitation, electro-chemical separation, ion exchange membrane filtration, solvent extraction, reverse osmosis and adsorption.[3–5] Among these,

adsorption is the most effective technique for Hg(II) removal whereas other methods are limited due to excessive time requirements, high costs and the production of highly toxic sludge. In recent years, low-cost adsorbents that have metal-binding capacities have become one of the alternative treatments for the removal of heavy metals. The adsorbents may be industrial by-products, agricultural wastes, biomass or polymeric materials.[6–8] Functional groups, such as carboxylate, hydroxyl, sulfate, amide and amino groups appended onto the adsorbents were responsible for metal binding. However, since the effective density of these groups for metal binding is generally low, most lignocellulosic adsorbents do not show a high sorption capacity. Thus to improve the adsorption capacity of lignocellulosic adsorbents, various physical or chemical surface treatments have been explored.

Graft copolymerization has been considered to be a powerful method for surface modification of lignocellulosic fibers. In graft copolymer synthesis, there are various methods for the generation of free radical sites on preformed polymer (poly-saccharide in case of grafted polysaccharides). Conventional non-chemical radical initiators, high energy radiation (gamma rays or electron beam), UV rays in the presence of photo sensitizers or microwave radiation are used for this purpose.[3,9–11] Conventional non-chemical radical initiators essentially require an inert atmosphere and control of the percentage grafting and reproducibility is quite low.[12] Microwave-based synthesis of graft copolymers has the inherent advantage of being fast, simple, highly reproducible and

[a]Department of Chemistry, Faculty of Science, Universiti Teknologi Malaysia, UTM, 81310 Johor Bahru, Johor, Malaysia. E-mail: sugeng@utm.my

[b]Centre for Sustainable Nanomaterials, Ibnu Sina Institute for Scientific and Industrial Research, Universiti Teknologi Malaysia, UTM, 81310 Johor Bahru, Johor, Malaysia

[c]Department of Chemical Engineering, Faculty of Chemical and Energy Engineering, Universiti Teknologi Malaysia, UTM, 81310 Johor Bahru, Johor, Malaysia

[d]Centre of Hydrogen Energy, Institute of Future Energy, Universiti Teknologi Malaysia, UTM, 81310 Johor Bahru, Johor, Malaysia

[e]Malaysian Nuclear Agency, Radiation Processing Technology, Bangi, 43000, Kajang, Selangor, Malaysia

[f]Department of Chemistry, Institut Teknologi Sepuluh Nopember, Keputih Sukolilo, Surabaya 60111, Indonesia

† Electronic supplementary information (ESI) available. See DOI: 10.1039/c6ra03741k

providing a great degree of control over percentage grafting. However, Mishra *et al.*, reported that grafting reaction initiated by a combination of microwave radiation and conventional method will yield grafted products with a higher percentage of grafting. Thus, in the microwave-based synthesis method, it is necessary to utilize a non-chemical radical initiator to enhance the formation of radical sites on the backbone of cellulose. Among different innovative techniques used for the production of sorption-active materials, the application of economical and ecologically clean radiation technologies is now under the attention of researches. In particular, the utilization of the electron beam-radiation-induced graft polymerization technique allows the inert polymeric matrix and the chains of a monomer with desirable functional groups to be introduced, or the chains of a precursor-monomer to be grafted, which can be subsequently modified.

In this study, banana stem fibers (BSF) were used for surface modification to enhance Hg(II) adsorption. Banana stem is one of the plant residues that is commonly available and by far one of the most abundant sources of cellulose.[4] Methacrylic acid, with a –COOH functional group, was grafted onto BSF using various free radical generation methods (β-radiation, microwave radiation and conventional chemical initiator). The functional and surface chemistry of the grafted fibers were analyzed. The adsorption capacity of the adsorbents was tested for the removal of Hg(II) from aqueous system. The Hg(II) adsorption capacity onto grafted BSF increased in the following order: BSF-β > BSF-MW > BSF-C. Moreover, adsorption equilibrium isotherms, kinetics and thermodynamic studies indicated that the nature of Hg(II) adsorption onto BSF-β is endothermic, non-spontaneous and adsorbed on the heterogeneous surface of the adsorbent. Thus, efforts have been made to convert this agricultural waste into inexpensive and effective material for industrial purposes.

Experimental

Materials

BSF were extracted from the pseudostem of banana plant which was collected in Johor Bahru (Malaysia) area. Methacrylic acid (MAAc) was used as monomer. Potassium peroxodisulphate, KPS ($K_2S_2O_8$) was used as initiator. Mercury chloride ($HgCl_2$) was used in adsorption experiments. All the chemicals were used as received without further treatment.

Preparation of BSF

The BSF was prepared by a simple pre-treatment according to the previous report.[13] Briefly, after delignification process, 3 g of dried BSF was treated with 0.1 M HCl followed by washing until pH 7, drying overnight at 373 K and stored in a vacuum desiccator. After pre-treatment, the BSF was composed mainly of cellulose, hemicellulose and lignin with 88.3, 6.98 and 4.71%, respectively.

Grafting BSF by β-radiation method

MAAc was dissolved in distilled water with 10% v/v of concentration. Glass containers were filled with this solution and

deoxygenated using N_2 bubbling for 5 min. 1 g of BSF was immersed in this solution and the mixture was deoxygenated again for another 10 min. The samples were irradiated by electron beam (β-radiation) at voltage of 2 MeV and current 10 mA at doses ranging from 20 to 80 kGy. The irradiated sample was left in temperature-controlled water bath for reaction at predetermined period of time. The homopolymers and unreacted monomers were removed by washing repeatedly with isopropyl alcohol (IPA) solution. The samples were then dried at 333 K for 24 h and referred as BSF-$β_x$ (x = adsorbed dose). The grafting yield or percentage grafting (%DG) was calculated using the equation below:

$$\%DG = \frac{W_g - W_i}{W_i} \tag{1}$$

where, W_g and W_i are the weights of grafted and/or crosslinked BSF and ungrafted BSF, respectively.

Grafting BSF by microwave method

1 g of BSF was immersed in 20 mL of 10 wt% MAAc and irradiated in a domestic microwave oven (Samsung, MW71C) for 6 min. The microwave power was varied from 300–800 W in order to investigate the efficiency of grafting. After the completion of reaction time, the product obtained was washed with IPA solution and distilled water and dried at 333 K and referred as BSF-MW_x (x = microwave power). The grafting yield (%G) was calculated using eqn (1).

Grafting BSF by conventional method

1 g of BSF was immersed with 20 mL distilled water in a 50 mL R.B. flask. The predetermined quantity of KPS initiator was added to the reaction mixture and allowed to interact for 10 min to facilitate free radical formation on the cellulose backbone under nitrogen atmosphere. Desired amount of MAAc (10% v/v) was added to the mixture and grafting was allowed under refluxed for 2 h at 343 K. The product obtained was filtered off, washed by IPA solution and distilled water several times until pH 7, finally dried at 333 K and referred as BSF-C_x (x = concentration of initiator). The grafting yield (%G) was calculated using eqn (1).

Characterization of adsorbent

The X-ray diffraction (XRD) patterns of the adsorbents were recorded on a Bruker AXS D8 Automatic Powder Diffractometer using Cu Kα radiation with $λ = 1.5418$ Å at 40 kV and 40 mA in the range of $2θ = 8–56°$. The Segal's empirical method[14] was used to obtain the crystallinity index of the samples X_c, as shown in eqn (2):

$$X_c = \frac{I_{002} - I_{am}}{I_{002}} \times 100 \tag{2}$$

where I_{002} and I_{am} are the peak intensities of crystalline and amorphous materials, respectively.

Infrared spectra of the adsorbents were obtained using a Fourier transform infrared spectrometer (Agilent Cary 640 FTIR spectrometer) in the range of 450–3650 cm^{-1}. The sample

was finely ground and dispersed into KBr powder-pressed pellets using a ratio of approximately 0.001 g sample/0.1 g KBr.

Electron spin resonance (ESR) provides signals corresponding to free radicals and/or paramagnetic ions, which is a count of the number of unpaired electrons (spins) available in a sample. ESR study was conducted using a JEOL JES-FA100 ESR spectrometer at room temperature. Prior to the analysis, the sample was outgassed at 373 K for 1 h for activation of adsorbent.

Thermogravimetric (TGA) analysis was carried out with a Mettler Toledo TGA/SDTA851. Approximately 8 mg sample was heated from 300 to 1023 K at 10 K min^{-1}, under flow of N_2 (20 mL min^{-1}).

In swelling studies, the dry samples of ungrafted and grafted BSF were soaked in distilled water for 24 h at room temperature. The samples were then taken out and excess solvent was removed by pressing between the folds of the filter paper. The samples were weighed again to obtain the final weight. The degree of swelling (%S) was calculated as follows:

$$\%S = \frac{W_f - W_i}{W_i} \times 100 \qquad (3)$$

where, W_i is the initial weight of the dried fiber and W_f is the final weight after the swelling.

The zero point charge (pH_{zpc}) of the BSF was determined using a powder addition method.[15]

Adsorption experiments

Batch adsorption experiment was conducted by adding 0.01 g adsorbent in a 200 mL of 20 mg L^{-1} Hg(II) solution. The Hg(II) solution was prepared by dissolving $HgCl_2$ in double distilled water. Prior to the adsorption, the adsorbent was activated *in vacuo* at 373 K for 1 h. The pH of the working solutions was adjusted to the desired value with 0.1 M HCl or 0.1 M NaOH. The mixture was incubated with a constant stirring rate of 300 rpm at room temperature to reach equilibrium. The adsorption isotherm experiment was conducted at 303 K with the concentration varying from 10 to 150 mg L^{-1}, while the kinetic and thermodynamic experiments were conducted at 303–333 K with a constant initial Hg concentration (20 mg L^{-1}). The values of kinetic and isotherm parameters were determined by a non-linear regression analysis using GraphPad PRISM 6 software. The sampling was taken at appropriate time intervals and followed by centrifugation at 14 000 rpm for 15 min. The residual Hg(II) concentration was determined with an Agilent 4100 MP-AES spectrometer.

Regeneration and reuse of adsorbents

To investigate the possibility of repeated use of the adsorbent, regeneration and reusability experiments were also conducted. The Hg(II)-loaded BSF-β_{40} was filtered and Hg(II) content in the solution was measured. The spent BSF-β_{40} was then transferred to another conical flask and stirred with 50 mL of 0.1 M HCl solution for 4 h at room temperature.[16] It was again filtered and the spent BSF-β_{40} was washed several times with distilled water followed by drying in oven at 333 K for overnight and used for

next adsorption cycle. The adsorption and desorption procedures were repeated using the same adsorbent.

Results and discussion

Characterization of adsorbents

The X-ray diffraction (XRD) patterns of BSF adsorbents are presented in Fig. 1A. The XRD patterns of ungrafted and grafted BSF exhibited mainly the cellulose I structure which consists of two distinct crystal phases, namely I_a and I_b. The major diffraction peaks at $2\theta = 16°$ and $21.9°$ are assigned to the crystallographic plane of the (101) and (002) reflection. The crystallinity indices for BSF, BSF-β, BSF-MW and BSF-C are 64.4, 18.1, 61 and 51.6%, respectively. An extensive decrease in the crystallinity was observed on BSF-β indicated modification was occurred in the crystal regions which destroyed the hydrogen bond effect; thus, more celluloses were exposed. This also implied that more cellulose could directly react with MAAc for the functional group being introduced easily.[17] Additionally, BSF-β showed broadening of the peak after grafting due to convergence of the fibers towards a more disordered system.[11] Wan *et al.*, reported a similar observation on methyl methacrylate grafted on bamboo cellulose, where the crystallinity was found to decrease after grafting due to the randomness of the amorphous phase in the graft copolymers.[18] Whereas grafted BSF prepared under the influence of microwave radiations showed fewer disturbances in the crystalline lattice. This is due to less surface deformations during grafting process under the influence of microwave radiations, thereby retaining better crystalline structure.[19] Furthermore, the XRD pattern of Hg-loaded BSF-β shows an amorphous structure which can be attributed to the destruction of inter- and intra-molecular hydrogen bonding between cellulose chains.[20,21]

Fig. 1B illustrates the FTIR spectra of BSF and grafted BSF with different preparation methods. All BSF possessed absorbance bands centered at 3405, 2877 and 1631 cm^{-1},
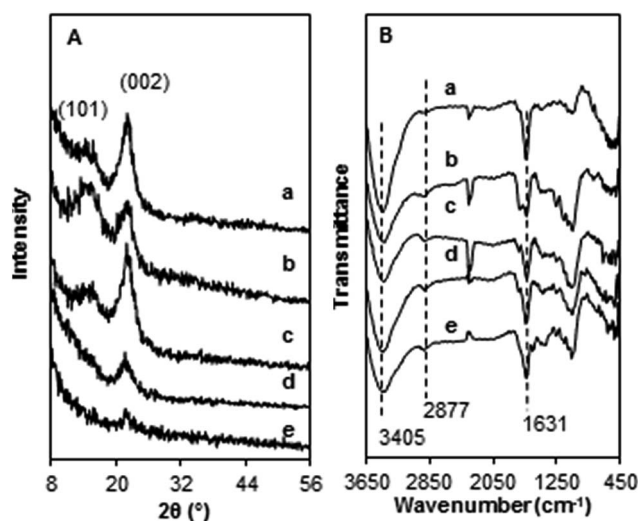
Fig. 1 (A) XRD pattern and (B) FTIR spectra of (a) BSF, (b) BSF-β, (c) BSF-MW, (d) BSF-C and (e) Hg loaded on BSF-β.

corresponding to OH groups from the glucosidic ring of cellulose, C–H stretching of the methyl and methylene groups and C=C stretching of methylene group, respectively. The bands in the region of 1030–1150 cm^{-1} are mainly attributed to the polysaccharide skeleton (including the vibrations of the glycoside bonds, C–O and C–O–C stretching vibrations).[22] In the case of all grafted BSF, additional peaks were observed at 1717 and 1664 cm^{-1} due to C=O stretching vibration, which confirms the grafting of MAAc onto BSF. In addition, the OH peak at the 4000–2995 cm^{-1} region becomes weaker and broader and shifts from 3405 to 3370 cm^{-1}. This may result from destruction of intermolecular and intramolecular hydrogen bonds by the graft reaction occurring in the hydroxyl groups.[23] The spectrum of Hg(II) loaded on BSF-β is also shown in Fig. 1B. The band at 1717 cm^{-1} attributed to the C=O from the carboxyl group was markedly decreased. The spectral analysis before and after metal binding indicates that the –COOH group was involved in metal adsorption. Fig. 2 shows the Gaussian-curve fitting for the FTIR spectra of raw and grafted BSF. Curve-fitting was performed with two Gaussian peaks located at 1717 and 1664 cm^{-1}. It could be noted that the peak areas of the C=O for BSF-β was the highest among all grafted BSFs, indicating that β-radiation produced more free radicals on cellulose backbone and initiated the graft-polymerization (Table S1†).

The presence of electron deficient oxygen (surface defects) formed after activation on all adsorbents is shown in Fig. 3A. The ESR signals for all grafted BSF were shifted from 1.9809 to 1.9802. This may be due to the abstraction of hydrogen atoms from two different species: (i) the hydroxyl group on the carbon of the cellulose and (ii) the carboxyl group from the methacrylic acid monomer. Similarly, according to Matsuda et al., two different EPR signals were observed in their catalyst which may be attributed to oxygen vacancy in different sites.[24] The electron deficient oxygen concentrations were shown by the relative signal strength which was determined by measuring the distance between the peak-to-peak values in the ESR spectra (Fig. 3B). The concentration of surface defects increased in the following order:
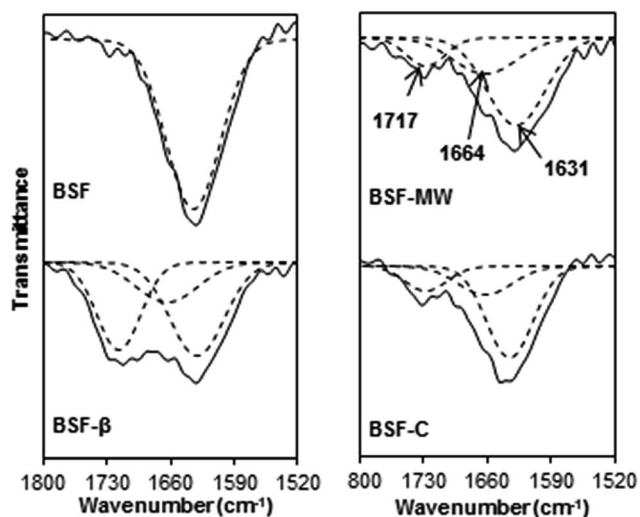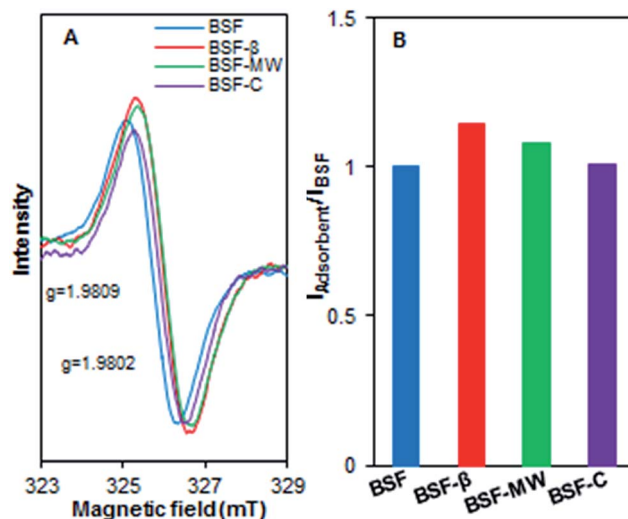
Fig. 3 (A) ESR spectra of BSF based adsorbents and their (B) variations in the intensity of the ESR signal at $g = 1.98$.

BSF-β > BSF-MW > BSF-C > BSF. This result indicates an increase of functional groups (–OH and –COOH) in the BSF structure which would be responsible for the increase in signal.

The TGA analysis of BSF, BSF-β, BSF-MW and BSF-C is presented in Fig. S1.† The initial decomposition temperature (IDT), final decomposition temperature (FDT) and decomposition temperatures per 10% weight loss are summarized in Table 1. Thermal behavior of both raw and grafted BSF was studied as a function of weight percentage residue with an increase in temperature. Three stages of thermal decomposition were observed for BSF. These decomposition stages began at 340 K (mass loss: 8%), 511 K (mass loss: 67%) and >700 K (mass loss: 20%). The first stage of decomposition in BSF may be associated with water desorption. In the second stage, maximum weight loss occurred, which may be due to the splitting of cellulose structure and chain scission evolving CO, CO_2 and the formation of carbonaceous residues.[22,25] Mass loss observed above 700 K was due to the oxidation of char. Grafted BSF had also undergone three stages of thermal decomposition. The first decomposition stage which occurred in the range of 341–347 K may be associated with the dehydration reactions. At a temperature of 500 K, the second stage of decomposition involved both depolymerization reactions and the breaking of crosslinks between polymers, as maximum weight loss (74%) was observed in this decomposition stage. The third and final stage of decomposition was observed above 790 K due to the decomposition of carboxyl groups and carbonization of poly(MAAc) acid chains. BSF-β exhibited IDT and FDT values of 486 and 749 K, respectively. The IDT of BSF-β was found to be much lower than that of BSF, whereas the FDT was found to be much higher (Table 1). The decrease in IDT of grafted BSF could be due to decomposition of anhydride of poly(MAAc) chains to CO_2 and intermediate species in the temperature range of 473–548 K. Furthermore, from the comparison of the decomposition temperatures per 10% weight loss, it is clear that the most marked weight loss occurred at higher temperatures for the

Fig. 2 Gaussian curve-fitting peaks of C=O for BSF based adsorbents.

Table 1 Thermogravimetric data of BSF, BSF-β, BSF-MW and BSF-C

| Sample | IDT (K) | DT (K) at every 10% weight loss | | | | | | | | Residue left (%) |
		20	30	40	50	60	70	80	90	
BSF	511	562	578	586	591	595	608	672	753	3
BSF-β	486	568	608	630	647	677	701	749	—	12
BSF-MW	509	573	599	614	626	636	648	696	—	11
BSF-C	509	571	595	611	622	631	641	702	—	10

grafted BSF than for the BSF. Higher DT and percent residue in case of the grafted BSF indicate an improvement in the thermal behavior upon grafting of MAAc onto BSF.[26,27]

Table S2† shows the swelling percentages of ungrafted and grafted BSF. The grafted BSF are BSF-β, BSF-MW and BSF-C which prepared at different irradiation dose, microwave power and concentration of KPS initiator, respectively. The ungrafted BSF possesses hydrophilic –OH groups at C2, C3, and C6 of the glucose unit, and hence has strong affinity with water. However for grafted BSF, the extent of interaction with water decreased as compared with ungrafted BSF. This may be due to the blockage of active sites on the main polymeric backbone by poly(MAA).[28] Apart from that, higher irradiation dose, microwave power and concentration of KPS initiator will enhanced the cross-linking process consequently hindered the diffusion and swelling properties by the network structure formation.[29].

Adsorption study

Effect of degree of grafting towards Hg(II) adsorption. Fig. 4 shows effect of degree of grafting towards the Hg(II) adsorption capacity using grafted BSF prepared by three different methods. The highest adsorption uptake was achieved using BSF-β_{40} with 73.4 mg g^{-1} followed by BSF-MW$_{600}$ (52.8 mg g^{-1}) and BSF-C$_{0.009}$ (39.4 mg g^{-1}). The highest Hg(II) adsorption for BSF-β_{40} may be due to the highest grafting percentage and amount of functional groups grafted on BSF as observed in FTIR and ESR

analyses. Due to this, further adsorption analyses were performed by using BSF-β_{40}, unless otherwise specified.

In the β-radiation-induced method, the irradiation dose is an important factor with which to optimize the grafting process and homogeneity of grafting distribution. The effect of adsorbed dose (20–80 kGγ) on the grafting yield of MAAc at a monomer concentration of 10% onto BSF was studied and shown in Fig. 4A. The grafting yield increased with increasing dose; it reached a maximum value of 79.2% at 40 kGγ. By further increasing the absorbed dose beyond 40 kGγ, the grafting yield was decreased. Also, as already known, graft polymerization is initiated by radicals which are produced by irradiation and radical reactions. Thus, the grafting yield depends on the amount of radicals formed in the system. However, radicals not only reacted with BSF but also with MAAc, creating grafting and homopolymer reactions. Based on the *Trommsdorff* effect, when an absorbed dose reaches above a certain value, a rapid transformation of monomers into homopolymers will reduce the mobility of the polymer chains and the grafting rate. At a higher adsorbed dose, the formation of homopolymers maybe favorable, which leads to a decrease in the grafting yield. Fig. 4A also showed the adsorption capacity (*q*) of BSF-β with different grafting yield. As can be seen, the adsorption capacity was dependent on grafting yield and the maximum adsorption capacity obtained was 73.4 mg g^{-1} at a maximum grafting yield of BSF. Further increasing the adsorbed dose led to a decrease
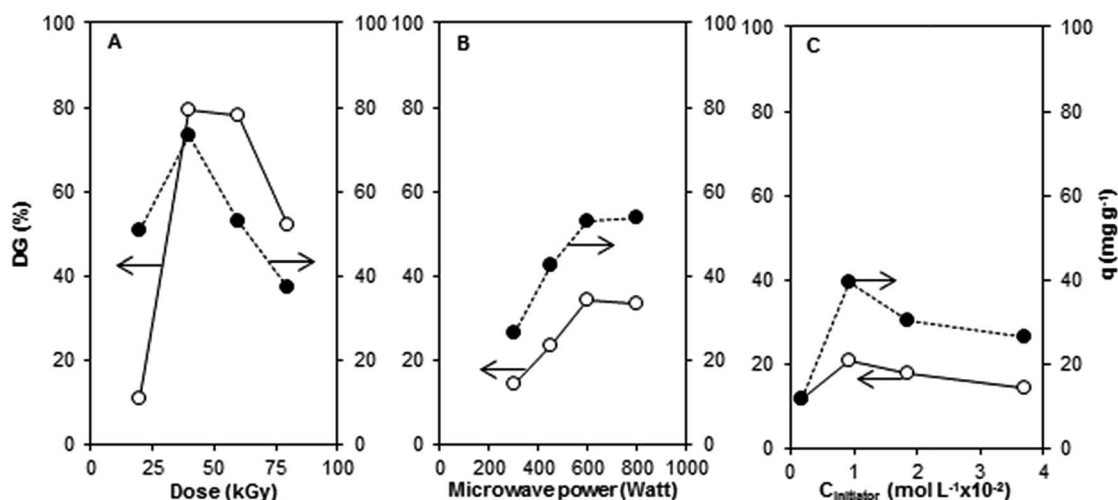
Fig. 4 (A) Effect of adsorbed dose of β-radiation, (B) microwave power and (C) initiator concentration on the degree of grafting and Hg(II) adsorption capacity.

in the grafting percentage and Hg(II) adsorption capacity. Interestingly, above the optimum radiation dose (>40 kGγ), the adsorption capacity did not decrease linearly with the grafting yield. For samples with higher grafting percentage, Hg(II) adsorption capacity was found to be lower than the expected value, which may be attributed to an increase in the cross-linking between monomers. As the degree of crosslinking increases, the metal complexation decreases due to a decrease in the available carboxylate ligands for metal binding.[7]

Fig. 4B demonstrates the degree of grafting for BSF-MW using microwave power ranging from 300 to 800 W and their adsorption capacity. The Hg(II) adsorption capacity using BSF-MW increased with a further increase in microwave power up to 600 W. This could be explained by an increase in the grafting percentage as power is increased, resulting from the generation of more macro radicals. However, beyond optimum value grafting percentage starts decreasing. This behavior may be due to either greater homopolymerization at high microwave power or decomposition of the graft copolymers.[30] The effect of KPS initiator concentration used during conventional method on the percentage of grafting and Hg(II) adsorption capacity are shown in Fig. 4C. The grafting percentage increased initially with an increase in the KPS concentration from 0.02×10^{-2} to 0.09×10^{-2} mol L^{-1}, with a maximum degree percentage of 20.6% achieved at the latter concentration. A further increase in the KPS concentration beyond 0.09×10^{-2} mol L^{-1} led to a decrease in grafting percentage. The initial increase in the grafting percentage was due to the generation of free radical sites on the cellulose backbone as a result of the increase in the total number of persulphate anionic radicals. The generation of active sites on the cellulose backbone was immediately followed by the grafting polymerization of MAAc onto the backbone. On the other hand, the decrease in grafting percentage beyond the optimum KPS concentration can be attributed to termination of the backbone radicals before grafting takes place due to the scavenging of the free radical sites on the cellulose backbone. Similarly, Hg(II) adsorption capacity increased as the grafting percentage increased and reached a maximum adsorption capacity at optimum KPS concentration with 39.4 mg g^{-1}.

Both grafted BSF prepared by microwave and chemical initiated method alone produced lower percentage of grafting and thus have lower adsorption capacities. In contrast, Mishra *et al.*, reported that graft polymerization by microwave radiation in synergism with a non-chemical radical initiator will generate more radical sites on cellulose backbone resulting in a higher percentage of grafting.[12] It is expected that higher Hg(II) adsorption capacity will be observed if there is presence of chemical initiator during microwave radiation in the graft polymerization process.

Scheme 1 represents the proposed reaction involved in the preparation of grafted BSF by three different methods (β-radiation, microwave radiation and conventional chemical initiator) for formation of free radicals on the cellulose backbone.[31–33] The radical sites then reacts with the methacrylic acid monomer, which is used to initiate graft copolymerization that initiate the graft polymerization. The highest grafting percentage was observed on BSF-β followed by BSF-MW and BSF-C. This result
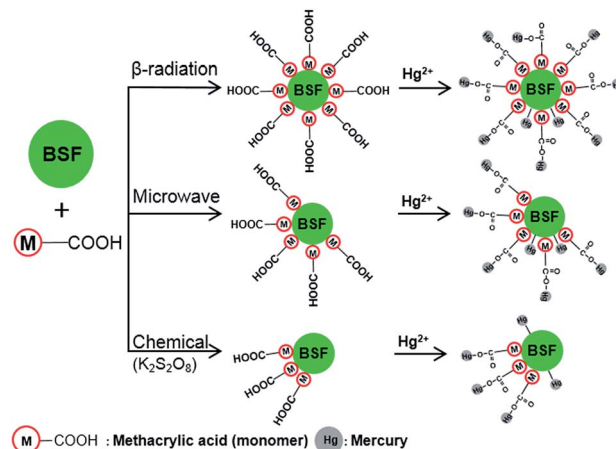
Scheme 1 Proposed grafting reaction of MAAc onto BSF by β-radiation, microwave radiation and conventional chemical initiator methods.

is in accordance with the FTIR and ESR analyses, where the carboxyl contents and surface defects increased in the following order: BSF-β > BSF-MW > BSF-C. The high grafting percentage will enhance the Hg(II) uptake due to higher number of available active adsorption sites.

Effect of pH. Initial pH of a solution may change the surface charge of an adsorbent, the degree of ionization of an adsorbate molecule and the extent of dissociation of functional groups on the active sites of an adsorbent. Therefore, experiment was performed in order to investigate the effect of pH on Hg(II) adsorption onto BSF-β_{40} by varying the pH from 2 to 11 (Fig. 5A). The Hg(II) adsorption capacity increased with increasing pH, reaching maximum uptake at pH 8 with 77.8 mg g^{-1}. As the pH value increases from 2 to 8, the deprotonation of COOH to COO− is favorable, leading to increase in the adsorption capacity.[34] Furthermore, a slight decrease in the equilibrium pH was recorded after adsorption (Fig. 5A). This indicates that as
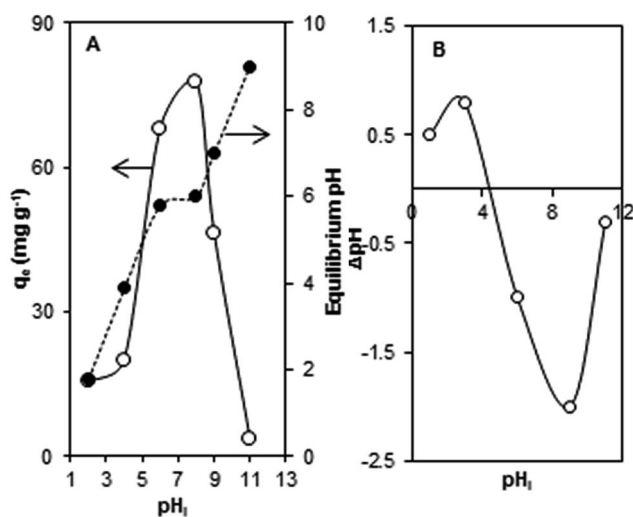
Fig. 5 (A) Effect of pH on Hg(II) adsorption onto BSF-β_{40} and (B) pH_{zpc} of BSF-β_{40}.

the metal ions are bound on the adsorbent, H^+ ions are released from the –COOH functional group into the solution and leads to the conclusion that BSF-β_{40} probably acts as an acid-form ion-exchanger.[35] The pH$_{zpc}$ of BSF-β_{40} as observed in Fig. 5B was found to be 4.5; below this pH, the surface charge of the adsorbent is positive. The uptake of metal ions in the pH range 2–7 is a H^+–M^{2+}/$M(OH)^+$ exchange process which also known as an electrostatic repulsion phenomenon. At low pH, the active sites of the adsorbent are less available for Hg^{2+} ions due to competition between the hydronium ions and the positively charged Hg ions for the surface adsorbing sites; subsequently, the adsorption of mercury ions will be low. At above pH$_{zpc}$, the Hg(II) adsorption capacity increased due to electrostatic attraction between positive sorbate species and negatively charged surface adsorbent. A decrease in the sorption at higher pH (above pH 8) is attributed to the formation of soluble hydroxyl complexes.[34]

Isotherm study

The equilibrium data were analyzed by non-linear regression method of two- and three-parameter isotherm models in order to examine the relationship between adsorption and aqueous concentration at equilibrium. The isotherm models, Langmuir, Freundlich, Temkin and Redlich–Peterson were used to describe the adsorption behavior of Hg^{2+} ions on the BSF-β_{40}; the equations used are as follows:

Langmuir:

$$q_e = \frac{q_m K_L C_e}{1 + K_L C_e} \quad (4)$$

Freundlich:

$$q_e = K_F C_e^{1/nF} \quad (5)$$

Temkin:

$$q_e = B_T \ln(A_T C_e) \quad (6)$$

Redlich–Peterson:

$$q_e = \frac{A_{RP} C_e}{1 + B_{RP} C_e^{\,g}} \quad (7)$$

where, q_e is the amount of Hg^{2+} ions adsorbed per gram of BSF-β (mg g^{-1}), q_m is the maximum adsorption capacity obtained from the isotherm (mg g^{-1}), C_e is the concentration of Hg^{2+} ions at equilibrium (mg L^{-1}), n_F is a heterogeneity factor, $B_T(RT/b_T)$, b (J mol^{-1}) is the heat of sorption, R is the gas constant (8.314 J mol^{-1} K^{-1}), T is the absolute temperature (K), and K_L, K_F and A_T are related to the constants of the Langmuir, Freundlich and Temkin, respectively. A_{RP} (L g^{-1}) and B_{RP} (L mg$^{-1(1-1/A)}$) are the Redlich–Peterson isotherm constants and g is the Redlich–Peterson isotherm exponent, which lies between 0 and 1. The non-linear isotherm fittings are shown in Fig. 6A, while the extracted isotherm information is summarized in Table 2. The applicability of the experimental data in fitting the equation isotherm models were determined by regression coefficient, R^2 and error function. Marquadt's percent standard deviation was employed as the error function and is given as below;
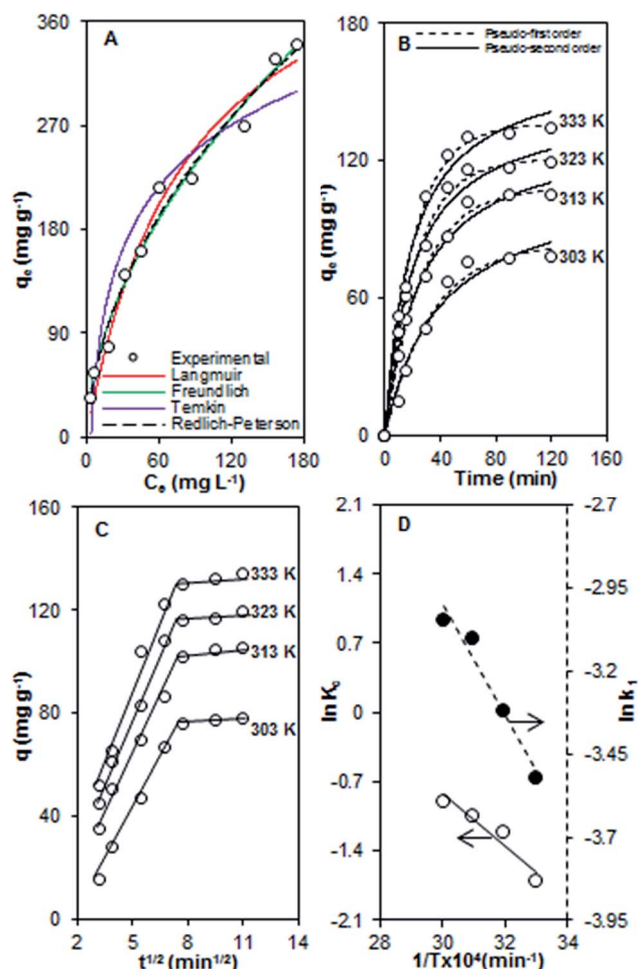
Fig. 6 Adsorption (A) isotherms, (B) kinetics, (C) intraparticle diffusion and (D) estimation of thermodynamic parameters (plot of ln K_c vs. 1/T) and activation energy (plot of ln k_1 vs. 1/T) for the Hg(II) adsorption onto BSF-β_{40}.

Table 2 Parameters of isotherm study for the Hg(II) adsorption on BSF-β_{40} at different Hg(II) initial concentration

Isotherm	Parameter	Value
Langmuir	q_m (mg g^{-1})	484
	K_L (L mg^{-1})	0.012
	R_L	0.957
	R^2	0.974
	MPSD	25
Freundlich	n	1.8
	K_F	20
	R^2	0.983
	MPSD	15
Temkin	A	0.27
	B	77.8
	R^2	0.917
	MPSD	50
Redlich–Peterson	A (L g^{-1})	23.8
	B (L mg$^{-1(1-1/A)}$)	0.742
	g	0.528
	R^2	0.984
	MPSD	14

$$\text{MPSD} = 100 \times \left(\sqrt{\frac{1}{p-n} \sum_{i=1}^{P} \left[\frac{(q_{e,meas} - q_{e,calc})}{q_{e,meas}} \right]^2} \right)_i \qquad (8)$$

where, p is the number of experiments and n is the number of parameters of a model equation. The adsorption capacity from the experimental data and from the model equation were denoted as $q_{e,meas}$ and $q_{e,calc}$, respectively. In the error estimation, the lower the MPSD value indicates better fit of the isotherm equations.[36] The coefficients and MPSD error values for all isotherm models are also listed in Table 2.

Among the three two-parameter isotherms tested, the result showed strong evidence that the Hg(II) adsorption onto BSF-β_{40} was best described by the Freundlich isotherm model with $R^2 = 0.983$. The Freundlich model suggested that an adsorption is described as occurring heterogeneously on adsorption sites due to numerous adsorbent–adsorbate interactions. The n_F obtained from this study was 1.8, which classified as favorable adsorption because $1 < n_F < 10$. A smaller value of n_F indicates better adsorption and the formation of a relatively strong bond between adsorbate and adsorbent.[37] A similar phenomenon has been observed by other researcher where adsorbent containing multifunctional groups such as –OH, –COOH and –SH were regarded as heterogenous.[3,31] However, the Langmuir isotherm could also be considered in estimating the maximum metal uptake values where they could not be reached in the experiments. The maximum adsorption capacity, q_m was 484 mg g^{-1}, which is better than ungrafted BSF and other adsorbents reported in the literature (Table 3). The dimensionless coefficient, R_L value was 0.957 showing that Hg(II) adsorption onto BSF-β_{40} is favorable. In contrast, a low R^2 value was obtained for Temkin isotherm when compared with the other two-parameter models. Hence, the experimental data could not be described by the Temkin model. The three-parameter isotherm, Redlich–Peterson model was analyzed using the equilibrium data to identify whether the isotherm approaches Freundlich or Langmuir. The constant g characterizes the isotherm as follows: if $g = 1$, the Langmuir will be the preferable isotherm, while if $g = 0$, the Freundlich isotherm will be the preferable isotherm. It is worth noting that the g value was not close to unity for Hg(II) adsorption on BSF-β_{40}, i.e., the data can preferably be fitted with Freundlich model. Furthermore, this model had the best fit with the experimental data due to the lowest MPSD error value (MPSD = 14) compared to other isotherm models.

Kinetic study

Adsorption kinetics describes the relationship of solute uptake rate of the adsorption and the adsorption time. The results obtained for the adsorption of Hg(II) onto BSF-β_{40} at different temperatures and contact time were analyzed by using non-linear regression method of pseudo-first order[38] and pseudo-second order[39] kinetic models.

The pseudo-first order kinetic equation based on adsorption equilibrium capacity is expressed in the following form:

$$q_t = q_e(1 - e^{-k_1 t}) \qquad (9)$$

while the pseudo-second order kinetic model can be written in the following form:

$$q_t = \frac{q_e^2 k_2 t}{1 + q_e k_2 t} \qquad (10)$$

where, q_t and q_e (mg g^{-1}) are the amounts of the Hg(II) ions adsorbed at time and equilibrium, respectively, while k_1 (min^{-1}) and k_2 (g mg^{-1} min^{-1}) are pseudo-first order and pseudo-second order rate constants, respectively.

The summary of the models used at four different temperatures and the kinetic information obtained from the pseudo-first and pseudo-second order plots are presented in Table S3.† Due to the closer value of adsorption uptake at equilibrium ($q_{e,calc}$) calculated from the pseudo-first order model with the experimental value compared to the pseudo-second order model, it could be concluded that the pseudo-first order kinetic model was the best fit for the experimental data, as shown in Fig. 6B.

In order to investigate the possible mechanism and rate controlling step of adsorption, the data were fitted with the Weber–Morris equation, which is the most commonly tested model.[40] The equation used is as follows:

$$q_t = k_{id} t^{1/2} + C_i \qquad (11)$$

where, k_{id} is a constant of intraparticle diffusion (mg g^{-1} min$^{-1/2}$), and C_i is the thickness of the boundary layer.

The plot of q_t against $t^{1/2}$ at different temperatures is shown in Fig. 6C. It can be seen that the plots were not linear over the entire time period, but could be divided into 2 parts, suggesting that two steps were involved in the adsorption process. The initial steeper line might be attributed to an external mass transfer of Hg^{2+} ions from the boundary layer to the surface of

Table 3 Comparison of adsorption capacity with other adsorbents

Adsorbent	Method of initiation	Adsorption capacity (mg g^{-1})	Ref.
BSF-β	β-Radiation	484	This study
BSF	—	372	13
Polyacrylamide grafted banana stalk	Chemical (FeAmSO$_4$)/H$_2$O$_2$	138	46
Carboxyl banana stem	Chemical CAN	90.88	33
Sugarcane bagasse cellulose modified with urea	Microwave	280	47
Polyacrylic acid grafted on *Cassia javanica* seed gum	Microwave	135	48
2-Mercaptobenzamide modified itaconic acid-grafted-magnetite nanocellulose composite	Chemical K$_2$S$_2$O$_8$	240	3

the BSF-β_{40} and the upper linear portion attributed to intra-particle diffusion. The initial external mass transport of Hg^{2+} ions was too rapid and then quickly slowed down, so that intraparticle diffusion became rate controlling. Table S3† shows the increasing trend of q_e, k_{id} and C_i as temperature increased. An increase in the temperature will increase the kinetic energy of Hg^{2+} species which will eventually cause faster diffusion and quicker adsorption. In addition, the intermolecular attraction and molecular association between the adsorbate and adsorbent at higher temperature will lead to a thicker boundary layer. This increment in boundary layer thickness with temperature supports the endothermic nature of the adsorption process.[41–43]

Thermodynamic study

The thermodynamic parameters, free energy of adsorption $\Delta G°$, entropy $\Delta S°$ and enthalpy $\Delta H°$ for the adsorption process by BSF-β_{40} were determined using Van't Hoff equation:

$$\Delta G° = -RT \ln K_c \quad (12)$$

$$\ln K_c = \frac{\Delta S°}{R} - \frac{\Delta H°}{RT} \quad (13)$$

where, $\Delta G°$ (kJ mol^{-1}) is the free energy change of specific adsorption, R is the universal gas constant (J K^{-1} mol^{-1}), T is the absolute temperature (K), K_c (L g^{-1}) is the equilibrium constant, $\Delta S°$ (J mol^{-1} K^{-1}) and $\Delta H°$ (kJ mol^{-1}) are the standard entropy and enthalpy changes of adsorption, respectively. The extracted thermodynamic information was summarized in Table S4.† The $\Delta G°$ values obtained were of positive values (4.3, 3.1, 2.8 and 2.5 kJ mol^{-1}) for the four temperatures (303, 313, 323 and 333 K). The positive values indicated that the adsorption process was a non-spontaneous process. The $\Delta S°$ and $\Delta H°$ parameters can be calculated from the intercept and slope of the plot of ln K_c vs. $1/T$, respectively (Fig. 6D). The positive value of $\Delta S°$ suggested the increasing randomness at the solid/liquid interface during the adsorption of Hg(II) onto BSF-β_{40}. The positive value of $\Delta H°$ (21.7 kJ mol^{-1}) indicated an endothermic adsorption process which was also supported by the increase in value of Hg^{2+} uptake with the rise in temperature. The endothermicity of the process also suggests that Hg(II) adsorption onto BSF-β_{40} appears to be controlled by chemical process.

The activation energy (E_a) is defined as the minimum kinetic energy required by the adsorbate ions to react with the active sites available on the surface of the adsorbent. The value of E_a can be obtained by the general Arrhenius equation.[44] The E_a value obtained from the slope of the plot of ln k_1 vs. $1/T$ (Fig. 6D) was 13.7 kJ mol^{-1}. It is noteworthy that low activation energies (<40 kJ mol^{-1}) are characteristic of physisorption, while higher activation energies (>40 kJ mol^{-1}) are indicative of chemisorption, and a range of 0.2 and 80 kJ mol^{-1} represents the ion exchange process.[45,46] The E_a value falls into the third range confirming that adsorption of Hg(II) onto BSF-β_{40} occurred in ion exchange process. This result is in accordance with the effect of pH analysis where BSF-β_{40} acted as acid-form ion-exchanger for Hg(II) adsorption. The positive value of E_a also suggests that a rise in temperature favors adsorption.

Comparison with other adsorbents

The maximum Hg(II) adsorption capacity (q_m) on BSF-β_{40} and other adsorbents reported in the literature are given in Table 3. It is evident that BSF-β_{40} demonstrated an outstanding Hg(II) removal capability with q_m higher than other adsorbents (484 mg g^{-1}). Previously, Shibi et al. reported the utilization of banana stalk for graft polymerization with acrylamide in the presence of a ferrous ammonium sulfate (FeAmSO$_4$)/H$_2$O$_2$ initiator system. Polyacrylamide-grafted banana stalk (PGBS) was able to adsorb mercury with maximum adsorption capacity, 138 mg g^{-1}.[47] Orlando et al. have studied the application of microwave radiation for the adsorption of mercury from the reaction of urea with the active sites present in sugarcane bagasse. This modification displayed an excellence result with maximum adsorption capacity of 280 mg g^{-1}; however, it needs longer time to achieve equilibrium.[48] Similar approach was conducted by Singh et al. where microwave induced poly(acrylic acid) grafted on *Cassia javanica* (CJ) seed gum revealed as an efficient Hg(II) adsorbent (q_m = 135 mg g^{-1}).[49] It was proved that method of initiation by high-energy radiation gave significant advantages over conventional method like high adsorption efficiency and free of initiator.

Effect of diverse ions and regeneration studies

Contaminated water often contains more than one heavy metal, which can potentially impact the adsorption behavior of each metal present as a result of competition among various ions present in the system. Other than mercury; arsenic, cadmium and lead are considered as the most toxic elements in wastewater. In order to evaluate the selectivity of BSF-β_{40}, experiments were carried out in different conditions; single, binary and quaternary mixtures of metal ions. The adsorption experiments were carried out at pH 6, with the presence of ions such as Pb(II), Cd(II) and As(v). The concentration of Hg(II) and each of the coexisting ions were maintained at 20 mg L^{-1}. As shown in Fig. 7A, the Hg(II) adsorption capacity was the highest in the single system, followed by binary and quaternary system. The adsorption capacity on BSF-β_{40} decreased by 31 and 23% in the presence of Pb(II) and Cd(II) cations separately; while no evidently competitive effects on the adsorption of Hg(II) was observed with the presence of As(v) anion alone. The significant interferences on Hg(II) adsorption by Pb(II) and Cd(II) may be due to their similar cationic structure with Hg in water environment. When comparing the binary systems Hg–Pb with Hg–Cd and Hg–As, the binding of Hg is more strongly influenced by Pb than by Cd or As, suggesting that the competition between Pb and Hg is stronger than between Hg and Cd or As.[50] In quaternary system, the adsorption affinity of Hg, Pb, Cd and As by BSF-β_{40} followed the order Pb(II) > Cd(II) > Hg(II) > As(v). It was reported in the literature that the higher the atomic size, electronegativity, electrode potential and ionic size, the greater will be the sorption affinity.[51] Furthermore, smaller metal ions has a larger hydration energy and thus less interacted with the adsorbent.[52] From this result, BSF-β_{40} is a diversified adsorbent which showed a high adsorption ability towards other heavy metals ions.
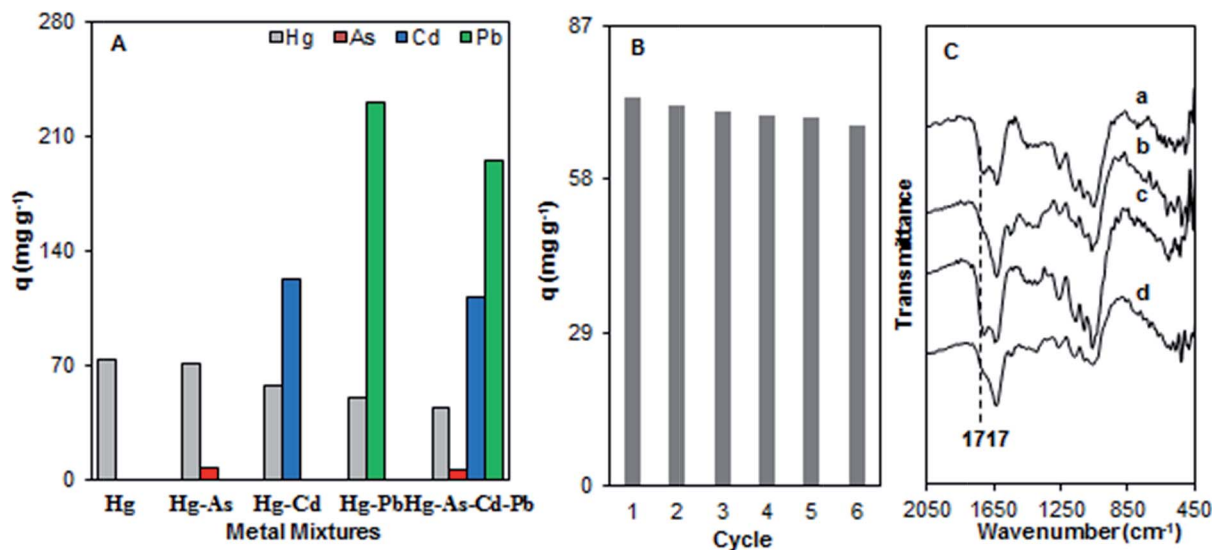
Fig. 7 (A) Effect of diverse ions on Hg(II) adsorption, (B) regeneration of adsorbent for Hg(II) adsorption and (C) FTIR spectra for (a) BSF-β40, (b) Hg loaded on BSF-β40, (c) BSF-β40 after desorbed and (d) Hg loaded on BSF-β40 after six cycles.

In order to make the adsorption process more economical, it is necessary to regenerate the adsorbent by a process called desorption. Therefore, adsorption–desorption studies were carried out with 0.1 M HCl as the eluted solution for six cycles; the results are shown in Fig. 7B. The adsorption capacity of BSF-β_{40} decreased from 73 to 68 mg g^{-1}, in an approximately 7% decrease during the six cycles. Additionally, more than 80% of the adsorbed Hg(II) ions were desorbed from the adsorbent. During desorption process using HCl solution, formation of chloro-complexes with Hg(II) ions are favorable and this is the main reason for the desorption of Hg(II).[53] Fig. 7C illustrated the FTIR spectra of BSF-β_{40}, Hg loaded on BSF-β_{40}, BSF-β_{40} after desorption and Hg loaded on BSF-β_{40} after six cycles. The band at 1717 cm^{-1}, which corresponded to C=O from the carboxyl groups, was observed after the desorption process (Fig. 7C, c). The results revealed that BSF-β_{40} was successfully regenerated with 0.1 M HCl and the functional groups were accessible for the next adsorption cycles. It is obvious that the spent BSF-β_{40} possessed high adsorption capacity, even after the six cycles, which can be repeated for multiple cycles. Thus regeneration of the adsorbent with 0.1 M HCl showed that the adsorption–desorption process using BSF-β_{40} was a reversible process.

Conclusion

This study demonstrated the ability of BSF-β with a carboxylate functional group to bind with Hg(II) ions from water. BSF was modified by grafting with methacrylic acid (MAAc) via three free radical generation methods (β-radiation, microwave radiation and non-chemical radical initiator). The β-radiation-induced method was found to be one of the best methods for modifying the surface of BSF due to the highest grafting percentage obtained as observed from FTIR and ESR analyses. The Hg(II) adsorption capacity increased in the following order: BSF-β_{40} > BSF-MW$_{600}$ > BSF-C$_{0.009}$. The adsorption isotherm results were well fitted to Freundlich model, which confirms the multilayer coverage of Hg(II) onto BSF-β_{40} owing to availability of multi-functional groups on BSF. The kinetic of adsorption follow pseudo-first order model. The activation energy (13.7 kJ mol^{-1}) confirmed that the adsorption of Hg(II) onto BSF-β_{40} occurred in ion exchange process which is in accordance with the effect of pH analysis where BSF-β_{40} acted as an acid-form ion-exchanger for Hg(II) adsorption. The thermodynamic studies provided evidence for non-spontaneity and endothermic nature of the adsorption process. A plant residue waste (BSF) was successfully transformed into a high capacity and low cost strong cationic polymeric adsorbent by using an environmental benign radiation-induced grafting process, which can be applied for heavy metal removal.

Acknowledgements

References

1 T. Kaghazchi and H. ShamsiJazeyi, *J. Ind. Eng. Chem.*, 2011, **17**, 608.

2 A. A. Ismaiel, M. K. Aroua and R. Yusoff, *Chem. Eng. J.*, 2013, **225**, 306.

3 T. S. Anirudhan and F. Shainy, *J. Colloid Interface Sci.*, 2015, **456**, 22.

4 V. S. Tran, H. H. Ngo, W. Guo, J. Zhang, S. Liang, C. Ton-That and X. Zhang, *Bioresour. Technol.*, 2015, **182**, 353.

5 U. Pancharoen, S. Sangtumrong, P. Ramakul, C. Satayaprasert and A. W. Lothingkum, *J. Ind. Eng. Chem.*, 2007, **13**, 751.

6 M. A. Z. Abidin, A. A. Jalil, S. Triwahyono, S. H. Adam and N. H. N. Kamarudin, *Biochem. Eng. J.*, 2011, **54**, 124.

7 D. Sud, G. Mahajan and M. P. Kaur, *Bioresour. Technol.*, 2008, **99**, 6017.

8 R. K. Gautam, A. Mudhoo, G. Lofrano and M. C. Chattopadhyaya, *J. Environ. Chem. Eng.*, 2014, **2**, 239.

9 N. K. Goel, V. Kumar, N. Misra and L. Varshney, *Carbohydr. Polym.*, 2015, **132**, 444.

10 H. Kang, R. Liu and Y. Huang, *Polymer*, 2015, **70**, A1.

11 E. S. Abdel-Halim and S. S. Al-Deyab, *React. Funct. Polym.*, 2014, **75**, 1.

12 S. Mishra, G. Sen, G. U. Rani and S. Sinha, *Int. J. Biol. Macromol.*, 2011, **49**, 591.

13 N. Salamun, S. Triwahyono, A. A. Jalil, T. Matsuura and N. F. M. Salleh, *RSC Adv.*, 2015, **5**, 14129.

14 L. Segal, J. J. Creely, A. E. Martin and C. M. Conrad, *Text. Res. J.*, 1959, **29**, 786.

15 A. Çelekli, M. Yavuzatmaca and H. Bozkurt, *Chem. Eng. J.*, 2009, **152**, 139.

16 R. K. Gupta, R. A. Singh and S. S. Dubey, *Sep. Purif. Technol.*, 2004, **38**, 225.

17 L. Zheng, C. Zhu, Z. Dang, H. Zhang, X. Yi and C. Liu, *Carbohydr. Polym.*, 2012, **90**, 1008.

18 Z. Wan, Z. Xiong, H. Ren, Y. Huang, H. Liu, H. Xiong, Y. Wu and J. Han, *Carbohydr. Polym.*, 2011, **83**, 264.

19 S. Kalia, S. Kumar and B. S. Kaith, *Malaysian Polymer Journal*, 2009, **4**, 46.

20 N. A. Abdelwahab, N. S. Ammar and H. S. Ibrahim, *Int. J. Biol. Macromol.*, 2015, **79**, 913.

21 G. Z. Kyzas, P. I. Siafaka, E. G. Pavlidou, K. J. Chrissafis and D. N. Bikiaris, *Chem. Eng. J.*, 2015, **259**, 438.

22 T. S. Anirudhan, A. R. Tharun and S. R. Rejeena, *Ind. Eng. Chem. Res.*, 2011, **50**, 1866.

23 X. Huang, X. Liao and B. Shi, *J. Hazard. Mater.*, 2009, **170**, 1141.

24 T. Matsuda, D. Nishimoto, K. Takahashi and M. Kimura, *J. Appl. Phys.*, 2014, **23**, 03CB03.

25 M. Gao and Q. Dai, *Chin. J. Process Eng.*, 2006, **6**, 242.

26 I. Kaur, V. Kumari, B. Sharma and N. Gupta, *Appl. Radiat. Isot.*, 2013, **79**, 118.

27 H. Mittal, R. Jindal, B. S. Kaith, A. Maity and S. S. Ray, *Carbohydr. Polym.*, 2015, **115**, 617.

28 V. K. Gupta, D. Pathania, B. Priya, A. S. Singha and G. Sharma, *Front. Chem.*, 2014, **2**, 1.

29 N. A. El-Kelesh and G. A. Mahmoud, *Cellul. Chem. Technol.*, 2015, **49**, 881.

30 V. K. Thakur, M. K. Thakur and R. K. Gupta, *Carbohydr. Polym.*, 2013, **97**, 18.

31 A. S. K. Kumar, M. Barathi, S. Puvvada and N. Rajesh, *J. Environ. Chem. Eng.*, 2013, **1**, 1359.

32 L. Wojnárovits, C. M. Földváry and E. Takács, *Radiat. Phys. Chem.*, 2010, **79**, 848.

33 A. S. Singha and A. Guleria, *Int. J. Biol. Macromol.*, 2014, **67**, 409.

34 T. S. Anirudhan, P. Senan and M. R. Unnithan, *Sep. Purif. Technol.*, 2007, **52**, 512.

35 G. Tan and D. Xiao, *J. Hazard. Mater.*, 2009, **164**, 1359.

36 K. Y. Foo, L. K. Lee and B. H. Hameed, *Chem. Eng. J.*, 2013, **223**, 604.

37 M. Zabihi, A. Haghighi Asl and A. Ahmadpour, *J. Hazard. Mater.*, 2010, **174**, 251.

38 S. Lagergren, *K. Sven. Vetenskapsakad. Handl.*, 1898, **24**, 1.

39 Y. S. Ho and G. Mckay, *Process Biochem.*, 1999, **34**, 451.

40 W. J. Weber and J. C. Morris, *J. Sanit. Eng. Div., Am. Soc. Civ. Eng.*, 1963, **89**, 31.

41 A. Fakhri, *RSC Adv.*, 2015, **5**, 2199.

42 A. E. Ofomaja, *Bioresour. Technol.*, 2010, **101**, 5868.

43 N. F. M. Salleh, A. A. Jalil, S. Triwahyono, J. Effendi, R. R. Mukti and B. H. Hameed, *Appl. Surf. Sci.*, 2015, **349**, 485.

44 K. J. Laidler, *J. Chem. Educ.*, 1984, **61**, 494.

45 V. J. Inglezakis and A. A. Zorpas, *Desalin. Water Treat.*, 2012, **39**, 149.

46 Z. Yu, T. Qi, J. Qu, L. Wang and J. Chu, *J. Hazard. Mater.*, 2009, **167**, 406.

47 I. G. Shibi and T. S. Anirudhan, *Ind. Eng. Chem. Res.*, 2002, **41**, 5341.

48 U. S. Orlando, A. U. Baes, W. Nishijima and M. Okada, *Green Chem.*, 2002, **4**, 555.

49 V. Singh, S. K. Singh and S. Maurya, *Chem. Eng. J.*, 2010, **160**, 129.

50 S. Ricordel, S. Taha, I. Cisse and G. Dorange, *Sep. Purif. Technol.*, 2001, **24**, 389.

51 M. Matouq, N. Jildeh, M. Qtaishat, M. Hindiyeh and M. Q. Al Syouf, *J. Environ. Chem. Eng.*, 2015, **3**, 775.

52 A. A. Taha, M. A. Shreadah, A. M. Ahmed and H. F. Heiba, *J. Environ. Chem. Eng.*, 2016, **4**, 1166.

53 T. S. Anirudhan, L. Divya and M. Ramachandran, *J. Hazard. Mater.*, 2008, **157**, 620.